Received: 13 February 2022 | Revised: 2 March 2022 | Accepted: 5 March 2022

DOI: 10.1002/ldr.4257

RESEARCH ARTICLE

WILEY

Heavy metal(loid)s in farmland soils on the Karst Plateau, Southwest China: An integrated analysis of geochemical baselines, source apportionment, and associated health risk

Jialiang Han[1,2] | Longchao Liang[3] | Yaru Zhu[4] | Xiaohang Xu[1,5] | Le Wang[6] | Lihai Shang[1] | Pan Wu[5] | Qixin Wu[5] | Xiaoli Qian[5] | Guangle Qiu[1] | Xinbin Feng[1]

[1]State Key Laboratory of Environmental Geochemistry, Institute of Geochemistry, Chinese Academy of Sciences, Guiyang, PR China

[2]University of Chinese Academy of Sciences, Beijing, PR China

[3]School of Chemistry and Materials Science, Guizhou Normal University, Guiyang, PR China

[4]College of Resource & Environment, Henan Agricultural University, Zhengzhou, PR China

[5]Key Laboratory of Karst Georesources and Environment, Ministry of Education, College of Resources and Environmental Engineering, Guizhou University, Guiyang, PR China

[6]Guizhou Province Key Laboratory for Information System of Mountainous Areas and Protection of Ecological Environment, Guizhou Normal University, Guiyang, PR China

Correspondence
Xiaohang Xu, State Key Laboratory of Environmental Geochemistry, Institute of Geochemistry, Chinese Academy of Sciences, Guiyang, 550081, PR China.
Email: xuxiaohang@vip.skleg.cn

Pan Wu, Key Laboratory of Karst Georesources and Environment, Ministry of Education, College of Resources and Environmental Engineering, Guizhou University, Guiyang 550025, PR China.
Email: pwu@gzu.edu.cn

Funding information
National Natural Science Foundation of China, Grant/Award Numbers: U1612442, 42003065; Ministry of Science and Technology of the People's Republic of China, Grant/Award Number: 2020YFC1808500; The Science and Technology Foundation of Guizhou Province, Grant/Award Number: Qiankehe[2020]1Y140; China Postdoctoral Science Foundation, Grant/Award Number: 2019M663571

Abstract

The Karst Plateau is characterized by elevated heavy metals (HM), the farmland soils in the Karst Plateau area is especially vulnerable to HM pollution. To cope with soil HM pollution and conduct precaution in Karst Plateau, the key bottleneck is to understand the pollution levels, sources, and priority-control of HM. Hence, geochemical baselines of HM in farmland soils were established to accurately evaluate the pollution characteristics. Pollution sources were identified with multivariate statistics, geostatistical methods, and receptor models. Priority-control of HM were distinguished via health assessments with a Monte Carlo simulation. A remarkable accumulation of Pb, Sb, Zn, As, and Cd was observed. Hotspots of As, Cd, Pb, Sb, and Zn clustered in the southwestern region of Hezhang. Pb–Zn related activities, cement product activities, coal mining, and coal combustion were dominant sources. Both noncarcinogenic risk and carcinogenic risk followed the order: children>adult females>adult males. As, Cd, and Pb were found to be priority contaminants in farmland soils in Hezhang.

KEYWORDS
exposure risks, geochemical baseline values, heavy metals, pollution characteristics, source apportionment

1 | INTRODUCTION

Heavy metals (HM) are highly toxic due to their ubiquitous persistence, non-biodegradability, and bioaccumulation in our surroundings (Yadav et al., 2019). As soil can serve as both a sink and a source for HM, thus, it plays an essential role in the cycle of HMs (Lian et al., 2019). HM contamination in farmland soils is especially important because HM not only reduce the soil quality but also endanger

human health through various pathways (Rinklebe et al., 2020). Hence, the increasing accumulation of HM in farmland soil poses a global challenge that has been attracting public concerns (Hu et al., 2020).

Given the high time and economic cost of remediation of HM-polluted soils, it is vital to conduct precautions to avoid further soil HM enrichment in farmland soils (Hu et al., 2016). Understanding the pollution levels, spatial patterns, and sources could instruct the prevention and reduction in new HM input (Hu et al., 2018; Jafarabadi et al., 2021). Pollution levels are usually obtained by comparing the actual concentration of pollutants with corresponding background values (BV) (Guan et al., 2019). However, spatial heterogeneity and extensive anthropogenic impacts make it difficult to accurately obtain these BV (Tian et al., 2017). Geochemical baseline values (GBV) of HM have been employed as a significant standard for soil quality assessment (Fernandez-Caliani et al., 2020). The BVs obtained from the GBV could discern the soil HM that were not influenced by anthropogenic activities (Guo, Wang, et al., 2021). Hence, GBV should be established to accurately characterize pollution levels.

Usually, the HM in soils primarily originate from natural and anthropogenic activities. In uncontaminated areas, HM derive from natural sources (Hu et al., 2020). Most HMs accumulation in farmland soils can be attributed to anthropogenic activities, including the application of agrochemicals (Zhao, Yan, et al., 2020), e-waste disposal (Luo et al., 2011), the atmospheric deposition from nonferrous HM mining and smelting (Jiang et al., 2021), fossil fuel combustion, vehicle emissions (Sun et al., 2019), and waste incineration (Li et al., 2015). Indeed, numerous efforts have been made to qualitatively identify the sources of HM in soils (Hou et al., 2017; Niu et al., 2013). Multivariate statistical analysis, including principal component analysis (PCA) and correlation analysis (CA), is widely employed to identify pollution sources (Long et al., 2021). Quantitative receptor models, positive matrix factorization (PMF), UNMIX, and absolute principal component analysis-multiple linear regression (APCS-MLR) can identify and quantify pollutant sources in the atmosphere, sediments, waters, and urban soils (Mehr et al., 2017; Mohammad et al., 2016; Sakizadeh & Zhang, 2021; Shen et al., 2021). Recently, receptor models have been successfully applied in quantifying pollutant sources in farmland soils (Zhang, Yan, et al., 2021). As different methods have their distinct characteristics, multivariate statistical analysis, geostatistical analysis, and receptor models were integrated to identify the sources of soil HM, providing more convincing results.

Human health risk evaluation is an important tool to distinguish the priority-control of HM. Traditional health exposure risk is usually obtained by some models with fixed parameters (Brtnický et al., 2019), biasing results of health risk evaluations due to individual variations (Hu et al., 2017; USEPA, 2001). Monte Carlo simulations (MCS) could reduce uncertainties by offering a health risk probability to HM (Hu et al., 2017). Hence, to distinguish priority-control HM, the probabilistic risk of HM has displayed an increasing trend.

The Karst Plateau region is one of the most ecologically fragile geomorphologic areas in the World (Zhan et al., 2021). The Southwest China karst region, the largest continuous karst terrain in the World, is characterized by elevated HM geological background values (Qin et al., 2021). Due to the shallowness of soils, low organic matter, and high pH, farmland soil in this karst region is sensitive to HM pollution (Liu et al., 2018; Liu, Wu, et al., 2020). Undoubtedly, this is even more so for farmland soils in the Karst Plateau, due to the much weaker capability of self-recovery. In the Karst Plateau, previous studies were mainly revealing the impacts of typical pollution sources, such as Pb–Zn mining and smelting sites (Duan et al., 2021; Xie et al., 2018). And the pollution status was only obtained by comparing with provincial BV (Chen et al., 2020; Zhang, Zhang, & Huang, 2021). Therefore, farmland soils in the Karst Plateau deserve special attention with respect to HM pollution. Unfortunately, no related work has been conducted to reveal geochemical baselines, pollution source, and associated risk in the Karst Plateau. The lack of such knowledge hinders the implementation of risk management practices for the farmland soils in the Karst Plateau.

To address the knowledge gap, we undertook a comprehensive study in Hezhang County in the Karst Plateau. The objectives of this study were to: (1) quantify the pollution characteristics of HM by establishing local GBV of HM in farmland soils; (2) apportion pollution sources by multivariate analysis, geostatistical analysis, and quantitative receptor models; and (3) distinguish the high priority-control of HM by evaluating human health exposure risks with MCS.

2 | MATERIALS AND METHODS

2.1 | Study area

Hezhang County, characterized by karst landform, is located in northwestern Guizhou Province, Southwest China. The 3250 km^2 lies in the Yunnan-Guizhou Plateau, at approximately >2000 m above sea level. The climate is subtropical and humid with a mean temperature of 13.4°C and mean annual precipitation of 854 mm. Hezhang is known for its rich Pb and Zn deposits and coal resources (Yang et al., 2006). Numerous quarries are also widely distributed throughout the region (HZSY, 2017). Centuries of artisanal Pb–Zn smelting and mining activities prevailed until 2004 in southwestern Hezhang (Feng et al., 2004). Even in 2020, large amounts of coal (1110,000 tons) and iron ores (677,000 tons) were mined. Additionally, cement (536,000 tons), cast iron (303,000 tons), and Zn (2222 tons) were also produced (HZBS, 2020).

2.2 | Sampling procedures and analysis

Surface soil samples (0–20 cm, $N = 365$) were collected from farmlands across Hezhang County in September 2020 (Figure 1). Each sample was composed of three subsamples. After collection, all the samples were stored in polyethylene plastic bags, marked, and then transferred into the laboratory. In the laboratory, all the samples were freeze-dried for 48 hr (FDU-2110, EYELA, Japan), ground with a mortar and pestle, passed through a 200-mesh sieve, and then preserved in polyethylene bags for chemical analysis.

For HM analysis, approximately 0.05 g of the soil sample was weighed, placed in a teflon tube, and digested with a mixture of

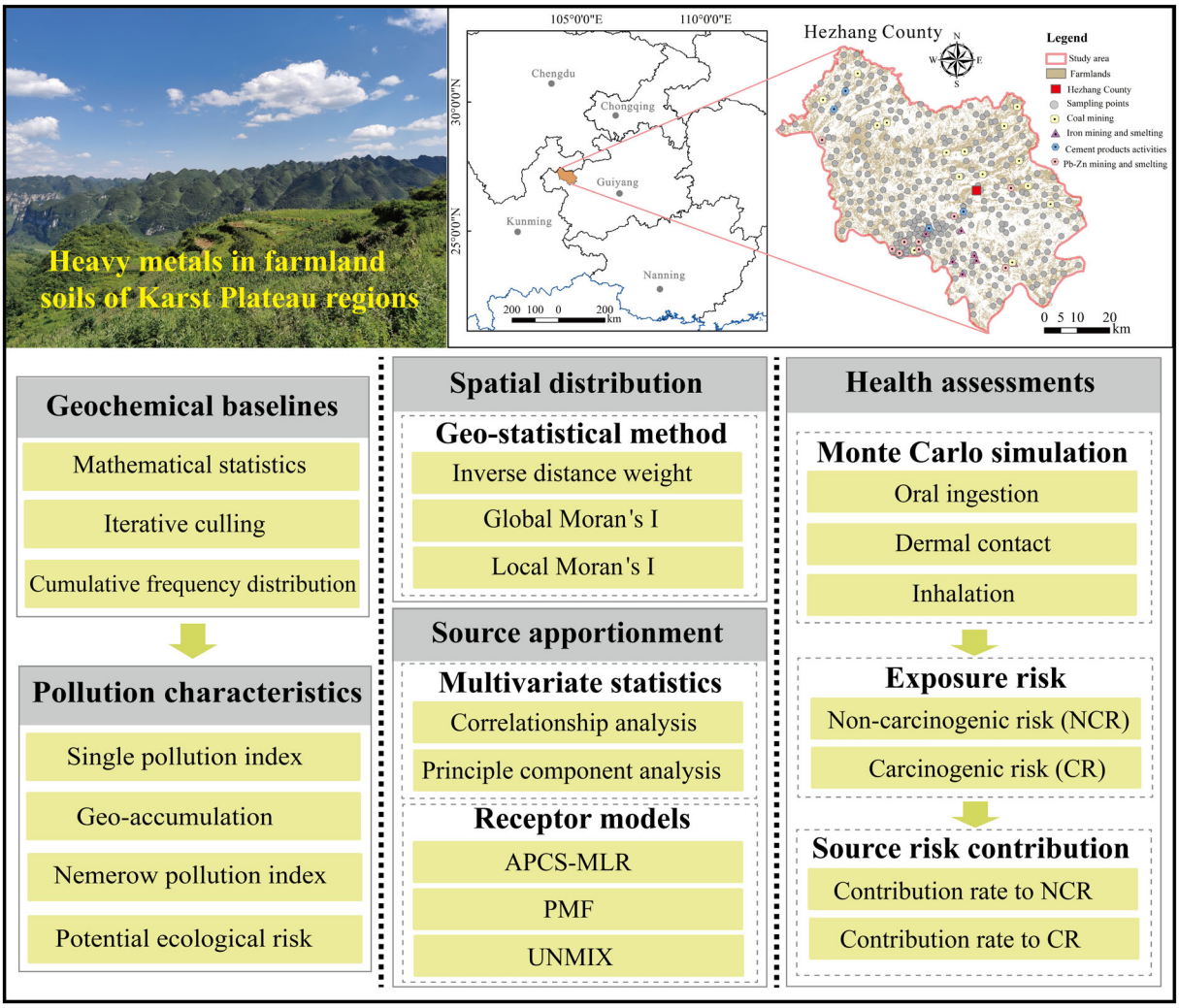

FIGURE 1 Sampling sites in the study area and the outlines of our study approach [Colour figure can be viewed at wileyonlinelibrary.com]

HNO_3 and HF at 160°C for 48 h. Once the tubes cooled to room temperature, the samples were evaporated to a nearly-dry state. Then, ultrapure water and HNO_3 were added and kept at 160°C for 16 hr. Finally, soil As, Cd, Cr, Cu, Mn, Ni, Pb, Sb, and Zn were obtained by inductively coupled plasma mass spectrometry (ICP-MS, NexION™ 300X, Perkin Elmer, USA).

The accuracy of the concentrations was guaranteed by the inclusion of internal standards. Chinese National Soil Reference Materials (GBW07405), duplicates, and reagent blanks were carried out. Around 93%–108% of the reference material was recovered, which was compatible with the certified values, within a relative standard deviation of less than 5%.

2.3 | Establishment of GBV

Calculating the GBV helps to identify the natural and anthropogenic sources of HM in soils. These values are also indicative of the level of HM pollution (Guan et al., 2019). The mathematical statistics (Cheng, Li, Li, et al., 2014), iterative culling (Wang et al., 2019), and the relative cumulative frequency distribution (CFD) (Wei & Wen, 2012) methods were employed to establish the GBV (see: Supporting information). Finally, the GBV were expressed as the mean values of these methods.

2.4 | Pollution status and ecological risk evaluation

To analyze the pollution characteristics, the single pollution index (P_i), the geo-accumulation index (I_{geo}), and the Nemerow pollution index (P_N) were adopted (Cheng, Li, Zhao, et al., 2014; Karim et al., 2015; Shaheen et al., 2020). Potential ecological risk of HM (E_r^i) to ecosystems was also assessed (Kamani et al., 2018). The corresponding details are shown in Supporting information.

2.5 | Spatial distribution

Color surface maps (Figure 3) of spatial distribution in the concentrations of HM were visualized with the inverse distance weighted (IDW) method in ARCGIS 10.4 (Esri, Redlands, CA). The IDW is on the

assumption that the predictions are a linear combination of available data:

$$Z(x) = \sum_{i=1}^{n} w_i z_i / \sum_{i=1}^{n} w_i, \quad (1)$$

$$w_i = d_i^{-u}, \quad (2)$$

Where: $Z(x)$ represents predicted value, Z_i is at a known point, n is the total size of known points used in interpolation, d_i denotes the distance from point i to the prediction point, and w_i is the weight assigned to point i. The detailed steps to obtain the spatial distribution map are shown in Figure S1.

2.6 | Moran's I

Moran's I, including global and local Moran's index, was applied as the indicator of spatial autocorrelation (Zhang et al., 2019). The global Moran's I could characterize the whole range from perfect negative spatial autocorrelation (−1) to perfect positive spatial autocorrelation (+1), respectively. When Moran's I approached 0, it indicates a lack of spatial autocorrelation. The local Moran's I describes the degree of local aggregation and differentiation between samples in space (Yuan et al., 2018).

$$\text{Global Moran's I} = \frac{\sum_{i=1}^{n}\sum_{j=1}^{n}(x_i - \bar{x})(x_j - \bar{x})}{S^2 \sum_{i=1}^{n}\sum_{j=1}^{n} w_{ij}}, \quad (3)$$

$$\text{Local Moran's I} = \frac{(x_i - \bar{x})}{S^2} \sum_{j=1}^{n} w_{ij}(x_j - \bar{x}), \quad (4)$$

Where: n represents the sampling size; x_i and x_j represent the measured values of sampling sites i and j, respectively; $\bar{x}$ refers to the mean value of x, S^2 denotes the variance of samples; and w_{ij} represents the distances between sites i and j. The spatial autocorrelation, obtained as the global Moran's I and local Moran's I, was gathered using ARCGIS 10.4 and GEO DA (http://geodacenter.github.io/). The detailed steps to obtain the spatial autocorrelation maps (both the global and local Moran's I) are shown in Figure S1.

2.7 | Source apportionment

PCA and CA were used to initially identify the dominant sources, and then receptor models were applied to quantitatively identify the sources.

2.7.1 | APCS-MLR

Kaiser–Meyer–Olkin (KMO) and Bartlett's sphericity tests were adopted to assess if the dataset was appropriate for PCA. Normalized factor scores and eigenvectors were used to conduct APCS-MLR to quantify sources (Guo et al., 2004). All potential sources were assumed to be linearly correlated with the final input pollution at the recipient site.

$$Z_{i,k} = \frac{(C_{i,k} - \mu_i)}{\sigma_i} \quad (5)$$

Where: $C_{i,k}$ indicates the concentration of the individual element i at location k, and μ_i and σ_i denote the mean concentration and the standard deviation of element i in all samples, respectively. Next, the following equations were used:

$$(Z_0)_k = \frac{(0 - \mu_i)}{\sigma_i} = -\frac{\mu_i}{\sigma_i}, \quad (6)$$

$$(A_0)_f = \sum_{i=1}^{i} S_{fi}(Z_0)_i, \quad (7)$$

Where: $(A_0)_f$ refers to the score of the principal component when the concentration is zero, and Z_0 and S denote the standard values when the concentrations are set to zero and the factor score coefficient, respectively. The scores of the absolute principal component (APCS) were calculated according to the following equation:

$$\text{APCS}_f = (A_Z)_{if} - (A_0)_f, \quad (8)$$

Where: A_Z represents the standardized factor scores obtained by conducting a PCA on standardized scores. The estimation of source contribution to individual elements involved a multiple linear regression:

$$x_{ij} = \sum_{p=1}^{n} (APCS_p \times b_{pj}), \quad (9)$$

Where: b_{pj} denotes the coefficient of multiple regression of the p_{th} pollution source; and APCS_p refers to the APCS score. According to the APCS-MLR, the contribution rate of every source could be obtained as the mean of $\text{APCS}_p \times b_{pj}$. To circumvent this concern, all the negative values were transformed into positive values (Liu, Dong, et al., 2020).

2.7.2 | PMF model

The PMF model is a mathematical approach to quantify the contribution of sources to samples. PMF 5.0 could resolve the concentration matrix into two matrices: factor contributions and factor profiles. The factors were analyzed on the basis of the following equation (Guan et al., 2019).

$$x_{ij} = \sum_{k=1}^{p} g_{ik} f_{kj} + e_{ij}, \quad (10)$$

Where: x_{ij} indicates the concentration of HMs, i represents the sample number, j denotes the chemical species, p refers to the source number, e denotes the error of each sample, u refers to the uncertainty calculated with the following equations:

$$\text{For } x_{ij} \le \text{MDL}, \quad u_{ij} = \frac{5}{6} \times \text{MDL}, \tag{11}$$

$$\text{For } x_{ij} > \text{MDL}, \quad u_{ij} = \sqrt{(\sigma \times x_{ij})^2 + (0.5 \times \text{MDL})^2}, \tag{12}$$

Where: MDL refers to the method detection limit of each element, and σ refers to the relative standard deviation.

2.7.3 | UNMIX

In UNMIX model, the singular value decomposition technique was employed to reduce the dimensions and determine the source numbers. The source contributions could be modeled by the following equation (Li et al., 2021):

$$x_{ij} = \sum_{l=1}^{p} \left(\sum_{k=1}^{p} U_{ik} D_{kl} \right) V_{lj} + \epsilon_{ij}, \tag{13}$$

Where: x_{ij} refers to the concentration of HM; U, D, and V represent the n × p, p × p, and p × m matrices, respectively; ϵ_{ij} indicates the error term comprising variability in x_{ij}, which is not considered by the first *p* principal component (Li et al., 2014).

2.8 | Health exposure risk

Oral ingestion, inhalation, and dermal contact are the major pathways of exposure to HM. These have been considered and calculated based on the risk assessment models recommended by the USEPA (Wang et al., 2020). The exposure risks of NCR and CR were obtained by MCS using the CRYSTAL BALL software. The specific RfD and SF values for different HM are displayed in Table S1.

$$\text{ADD}^i_{\text{Ing}} = \frac{C_i \times \text{IR}_S \times \text{EF} \times \text{ED}}{\text{BW} \times \text{AT}} \times 10^{-6}, \tag{14}$$

$$\text{ADD}^i_{\text{derm}} = \frac{C_i \times \text{SA} \times \text{SL} \times \text{ABF} \times \text{EF} \times \text{ED}}{\text{BW} \times \text{AT}} \times 10^{-6}, \tag{15}$$

$$\text{ADD}^i_{\text{inh}} = \frac{C_i \times \text{IR}_a \times \text{EF} \times \text{ED}}{\text{BW} \times \text{AT} \times \text{PEF}}, \tag{16}$$

$$\text{HI} = \sum \text{HQ} = \sum \frac{\text{ADD}_{ij}}{\text{RfD}_{ij}}, \tag{17}$$

$$\text{TCR} = \sum \text{CR} = \sum \text{ADD}_{ij} \times \text{SF}_{ij}, \tag{18}$$

Where: $\text{ADD}^i_{\text{Ing}}$, $\text{ADD}^i_{\text{derm}}$, and $\text{ADD}^i_{\text{inh}}$ refer to the average daily intake dose of *i* via oral ingestion, dermal contact, and inhalation, respectively, HQ represents the average hazard quotient, while C_i refers to the concentration (mg kg^{-1}) of HM *i*. Other parameters are described in Table S2. The addition of one category of resident HQ procured a hazard index (HI), displaying the exposure risk (Wu et al., 2020). An HI or HQ >1 was indicative of a potential adverse health risk (Mohseni Bandpi et al., 2018). The summation of all the potential risks of individual CR yielded the TCR value (Huang et al., 2021). If the CR or TCR >1E-4, it indicated a CR; if the CR or TCR <1E-4, there is no significant CR; and if the CR or TCR <1E-6, there was a negligible risk (USEPA, 2009).

2.9 | Data processing and statistical analysis

All data were processed using Microsoft EXCEL 2016. SPSS 23 and Microsoft EXCEL 2016 were used to obtain the APCS-MLR calculations. ORIGIN 2021 was used to prepare the figures. The spatial interpolations (IDW) were performed in ARCGIS 10.4. The spatial autocorrelation (the global Moran's I and local Moran's I) was gathered using both ARCGIS 10.4 and GEO DA.

3 | RESULTS

3.1 | HMs in farmland soils

The K-S test results displayed that Cr and Cu followed a lognormal distribution, while the remaining HMs followed a skewed distribution (Table 1). The geometric mean values of Cr and Cu, and the median values of As, Cd, Mn, Ni, Pb, and Zn were 119 and 79.5 mg/kg, 21.0, 1.99, 1112, 62.4, 44.6, and 223 mg kg_{-1}. Except Sb, all the other HM were greater than their corresponding BV (Table 2).

3.2 | Establishments of GBV

The local GBV were established to accurately assess pollution evaluation (Table 2). Generally, the GBV of Cd, Cr, Cu, Mn, Ni, and Zn (Figure S2 and Table 2) were 2.47-, 1.12-, 2.16-, 1.36-, 1.54-, and 1.90-times greater than those of the Guizhou Province BV (CNEMC, 1990). The GBV were higher than those in the global continental crust (Wedepohl, 1995). Moreover, the GBV were higher than those obtained in Huainan, Ningbo, the Hexi Corridor, and Jieyang City in China (Jiang et al., 2020; Lu et al., 2021; Niu et al., 2019; Wang et al., 2020); and various parts of Europe (Mico et al., 2007). This confirmed the high BV of HM in this Karst Plateau region.

3.3 | Pollution levels

Pollution levels (P_i, I_{geo}, and P_N) of HMs were calculated on GBV. Pollution levels of different HMs followed the order of: Pb > Sb > Zn > As>Cd > Cu > Cr > Mn > Ni (Figure 2). Overall, the high P_i values (>1) of all HM suggested widespread pollution. The P_i values of Pb, Sb, Zn, As, and Cd were 19.6, 6.46, 6.14, 2.70, and 2.29, respectively. Notably, approximately 33.2% of Pb, 27.4% of Sb, 18.1% of Zn, 16.7% of Cd, 12.6% of As, and 10.4% of Cu were considered to be heavy contamination (Table S3). Results of P_N ranged widely from

TABLE 1 Concentrations of HM in soils from farmland in Hezhang County

Categories	As (mg kg^{-1})	Cd (mg kg^{-1})	Cr (mg kg^{-1})	Cu (mg kg^{-1})	Mn (mg kg^{-1})	Ni (mg kg^{-1})	Pb (mg kg^{-1})	Sb (mg kg^{-1})	Zn (mg kg^{-1})	pH
Arithmetic mean	48.1	3.74	136	102	1210	64.2	623	7.95	1160	6.77
Geometric mean	20.7	2.13	119	79.5	997	58.1	75.9	2.37	294	6.66
Median	21.0	1.99	115	82.0	1112	62.4	44.6	1.91	223	7.05
Standard deviation	262	7.47	79.4	81.5	777	27.7	3331	33.5	5385	1.17
Variation coefficient (%)	545%	200%	58.4%	79.8%	64.2%	43.2%	534%	421%	464%	17.3%
Skewness	18.1	6.79	2.12	2.97	3.00	0.877	10.1	12.3	8.52	−0.543
Kurtosis	340	53.5	6.19	18.6	21.6	1.93	122	184	78.2	−1.041
Range	4953	75.2	531	828	8414	193	47,420	544	61,594	4.060
Minimum	0.297	0.289	29.9	11.5	65.1	7.23	10.2	0.265	14.6	4.21
Maximum	4953	75.5	561	839	8479	200	47,430	544	61,609	8.27
Distribution	Skew	Skew	Lognormal	Lognormal	Skew	Skew	Skew	Skew	Skew	Skew

TABLE 2 Geochemical baselines derived from mathematical statistics, iterative culling, and CFD

Element	Mathematical statistics (mg kg^{-1})	Iterative culling (mg kg^{-1})	Cumulative frequency (mg kg^{-1})	Mean value of geochemical baselines (mg kg^{-1})	Guizhou geochemical baselines in Guizhou (mg kg^{-1}) (CNEMC, 1990)	The mean China geochemical baselines (mg kg^{-1}) (Wang et al., 2016)	The CGB high background baselines (mg kg^{-1}) (Wang et al., 2016)
As	21.0	16.3	16.0	17.8	20	9	14
Cd	1.91	1.93	1.06	1.63	0.659	0.137	0.197
Cr	120	105	100	108	95.9	53	68
Cu	79.5	61.4	66.3	69.1	32	20	27
Mn	1113	1114	1015	1081	794	569	725
Ni	62.4	61.6	57.2	60.4	39.1	24	31
Pb	42.1	26.2	27.1	31.8	35.2	22	28
Sb	1.79	0.997	0.889	1.23	2.24	0.73	1.08
Zn	220	181	165	189	99.5	66.0	84.0

0.621-'safe' to 1071-'heavily contaminated' (Figure S3). The mean potential ecological risk index (RI) was 475, with a wide range from 34.2 to 286,864. Moreover, the E_r^i values of Cd (68.8), Pb (98.0), and Sb (259) indicated the moderate potential ecological risk with Cd; considerable potential ecological risk with Pb; and high potential ecological risk with Sb (Figure S4 and Table S6).

3.4 | Spatial distribution

Generally, most HMs displayed a distinguished spatial difference in the study area (Figure 3). Notably, the hotspots of As, Cd, Pb, Sb, and Zn were mainly in the southwestern and middle parts of Hezhang County, showing a decreasing trend from the southwestern to the northern region. The global Moran's I values showed significant positive spatial autocorrelations for As, Cd, Cu, Mn, Ni, Pb, Sb, and Zn (-Figure S5), with Moran's I values of 0.414, 0.510, 0.274, 0.144, 0.238, 0.708, 0.586, and 0.590, respectively. Among them, Sb had the highest Moran's I value, and Ni had the lowest Moran's I value. Moreover, the z scores of As, Cd, Cu, Mn, Ni, Pb, Sb, and Zn were >2.58, with all $p < 0.01$. This indicated a positive correlation in their spatial autocorrelations. However, Moran's I value of Cr was 0.0897 (with $z = 0.264$ and $p = 0.791$), indicating random distribution of Cr (-Figure S5). The local Moran's I values of As, Cd, Cr, Cu, Mn, Ni, Pb, Sb, and Zn were 0.023, 0.397, 0.215, 0.127, 0.166, 0.203, 0.202, 0.110, and 0.326, respectively.

3.5 | Source apportionments

Overall, except for Cr and Ni, significant positive correlations were observed between all the other HMs (Figure S6). Strongly positive relationships were observed between the following pairs: As–Pb, As–Sb, Cd–Pb, Cd–Sb, Cd–Zn, Cr–Ni, Pb–Sb, Pb–Zn, and Sb–Zn ($r = 0.601$–0.941, $p < 0.01$). Moderate positive correlations ($r = 0.302$–0.499, $p < 0.01$) were found for As–Cu, As–Zn, Cu–Mn,

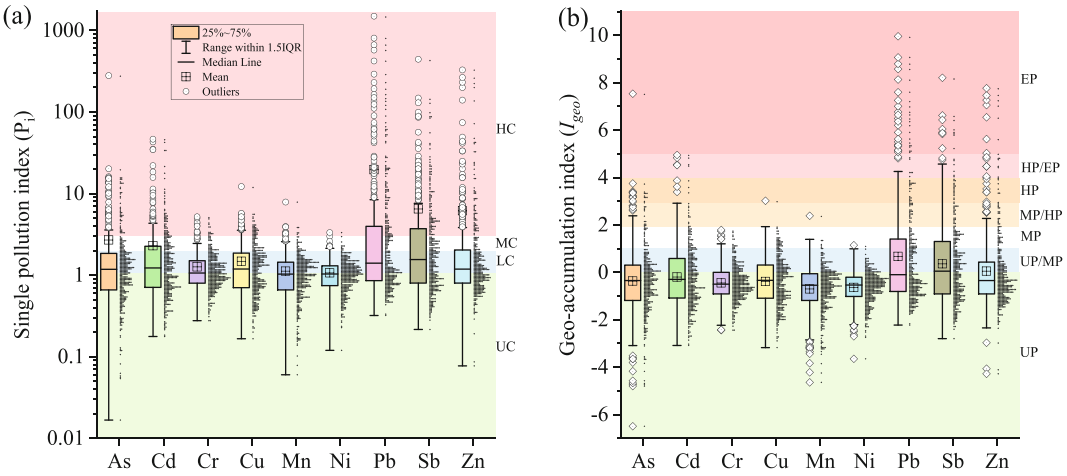

FIGURE 2 The values of single pollution index (P_i) (a) and geo-accumulation index (I_{geo}) (b) of different elements in soil samples. UC, uncontaminated; LC, low contaminated; MC, moderately contaminated; HC, high contaminated; UP, unpolluted; UP/MP, unpolluted/moderately polluted; MP, moderately polluted; MP/HP, moderately/heavily polluted; HP, heavily polluted; HP/EP, heavily polluted/extremely polluted; EP, extremely polluted [Colour figure can be viewed at wileyonlinelibrary.com]

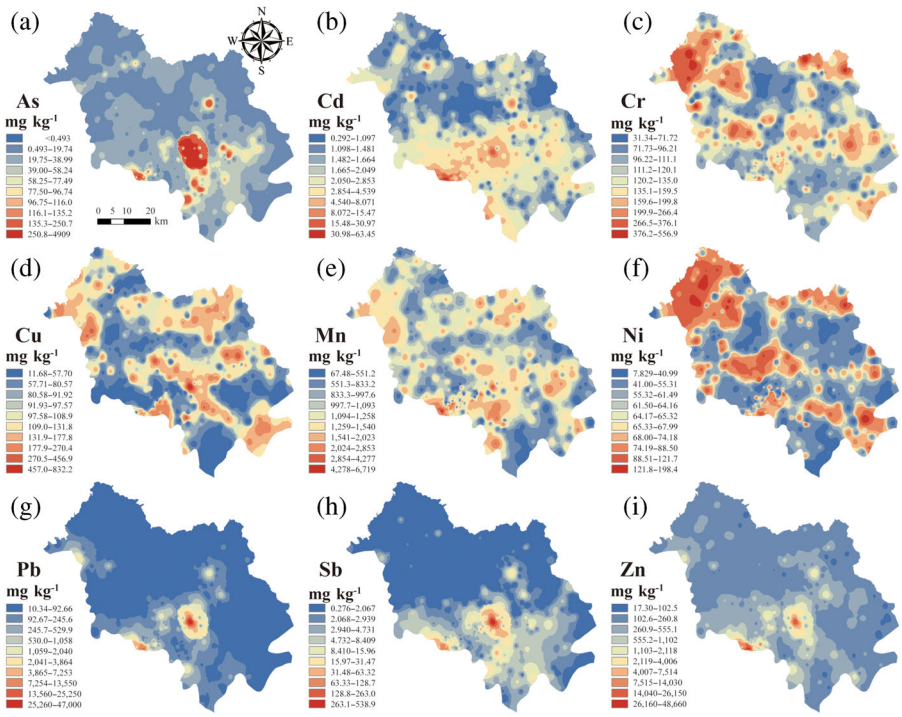

FIGURE 3 Spatial distributions of (a) As, (b) Cd, (c) Cr, (d) Cu, (e) Mn, (f) Ni, (g) Pb, (h) Sb, and (i) Zn [Colour figure can be viewed at wileyonlinelibrary.com]

Cu–Ni, Cu–Pb, Cu–Sb, Cu–Zn, Mn–Ni, and Mn–Sb. Significant correlations in these pairs indicated that these elements may share common sources (Guo, Wang, et al., 2021).

PCA yielded four principal components, whose eigenvalues were >1, accounting for 86.6% of the total data variance. Of them, PC1 explained 43.7% of the total data variance, mainly loaded with As, Cd, Pb, Sb, and Zn. PC2 explained 23.0% of the total data variance, loaded with high Ni (Table S7). The loadings of Cu and Mn were compatible in PC1 (0.555 and 0.658) and PC2 (0.658 and 0.401), respectively. PC3 explained 10.7% of the total variance, with the high loadings of Cr and Ni. Moreover, Ni had high loadings in both PC2 (0.721) and PC3 (0.541). Furthermore, PC4 explained 9.20% of the total variance and was only loaded with As. Results of CA and PCA were inconclusive, and receptor models were further employed to quantify the different sources of HM.

Factor 1 was primarily determined by Pb and Zn (Figure 5). Factor 2 was heavily loaded with Cu and Mn. Factor 3 is dominated by Cd accumulation, followed by Zn. F4 was dominated by Cr and Ni. Additionally, F5 was heavily loaded with As and Sb in results of PMF and UNMIX.

3.6 | Health exposure risks

In different groups (children, adult females, and adult males), the NCR and CR of residents' exposure to soil HMs via the three exposure pathways were calculated using MCS (Ginsberg & Belleggia, 2017; Xu et al., 2020). In contrast to adults, children were exposed to a higher NCR and CR, as the mean values of the HI and TCR displayed the order: children>adult females>adult males (Figure 6). And all the mean HQs were lower than 1. The mean HQs of all population categories in descending order are as follows: As > Pb > Cr > Sb > Mn > Cd > Ni > Cu > Zn. Generally, the high CR values of As, Cd, Cr, and Pb were above the acceptable threshold value of 1E-6 (Figure 7), implying a potential CR (Huang et al., 2021). Importantly, the mean CR of As in children (1.59E-4) was higher than the unacceptable threshold value (1E-4).

4 | DISCUSSION

4.1 | HM accumulation

Among these HM, the median value of Cd was above the risk screening value of 0.3 mg kg^{-1} but below the risk intervention value of 3 mg kg^{-1} (Table 1) (MEPRC, 2018). Considering the maximum values of As, Cd, and Pb were 41.3-, 25.2-, and 67.8-times higher than their corresponding risk intervention values, respectively (MEPRC, 2018). And the maximum values of Cr, Ni, and Zn were greater than the risk screening values of 200, 100, and 250 mg kg^{-1}, respectively. Pollution by these HM cannot be ignored. The high variation coefficients (>1) of As, Cd, Pb, Sb, and Zn (Table 1) implied a relatively high spatial variability and impacts from local anthropogenic activities (Wu et al., 2021). The Cd, Cr, Cu, Mn, Ni, and Zn values were higher than those in the karst region—Yunnan Province, Southwest China (Wang et al., 2021); and non-karst regions-Jieyang City, South China (Jiang et al., 2020); Aghili Plain and Tehran, Iran (Ahmadi et al., 2019; Hani & Pazira, 2011); and Alicante and Galicia, Spain (Franco-Uria et al., 2009; Mico et al., 2007); Jeddah City, Saudi Arabia (Balkhair & Ashraf, 2016). However, the As and Cd concentrations were lower than those in Ethiopia (Gebeyehu & Bayissa, 2020). The elevated coefficients of skewness for As, Pb, Sb, and Zn indicated that these four elements may be influenced by anthropogenic inputs (Table 1) (Li et al., 2020). The high kurtosis of As, Cd, Pb, Sb, and Zn suggested that bulks of the monitoring data clustered around their mean values (Jin et al., 2019).

For I_{geo}, the mean values of Pb (0.670), Sb (0.359), and Zn (0.0525) were positive, demonstrating that the soils of this study area were unpolluted to moderately polluted by these three metals (Figure 2b and Table S2). Notably, 37.5% of the samples were in the 'heavily contaminated' category (Table S5). These results suggested that the Pb, Sb, and Zn were more heavily contaminated than the other HMs. The mean values of E_r^i for HMs followed the order of Sb > Cd > Pb > As>Cu > Ni > Zn > Cr > Mn. Of these, Sb in the farmland soils had extremely high potential ecological risk; Cd and Pb had considerable potential ecological risk (Table S6). Approximately 11.8% of the total study sites had considerable potential ecological risk, 4.66% high potential ecological risk, and 6.30% extremely high potential ecological risk. Thus, Sb, Pb, and As were the main HM causing ecological risk in farmland soils, and several points may pose extremely high ecological risks.

4.2 | Spatial distribution of HM

As most of the hotspots were densely distributed in the middle-southwest part of the study area (Figure 3), in these parts, intensive industrial activities, including Pb–Zn mining and smelting, coal mining, and cement products activities (Briki et al., 2015), were distributed within the hotspots. The distribution of these peak values coincided with the distribution of intensive industrial activities (Figure 1), indicating industrial activities may be the key emission sources (Zhou et al., 2020). Furthermore, the prevailing northeasterly wind might prevent the migration of As, Cd, Pb, Sb, and Zn from southwestern to northern regions (HZSY, 2017). However, Cr, Mn, Ni, and Cu demonstrated different distribution characteristics with values peaking in the northwest, northeast, and the belt from the middle region to the southeastern edge (Figure 3), implying other pollution sources may act as key sources.

Results of the global Moran's I showed that most of them were spatial autocorrelated, which could instruct the pollution management in some typical pollution sites. The low-high sites were primarily located in the surroundings of the high-high sites, which was corroborated by previous studies (Jia et al., 2019; Tepanosyan et al., 2019). For As, Cd, Cu, Mn, Pb, Sb, and Zn, most of the high-high clustering were densely distributed in the southwestern part of Hezhang. This indicated that these HM may be dominated by similar sources (Wu et al., 2019). Actually, most Pb–Zn mining and smelting activities, as well as coal mining and iron smelting activities, were intensely distributed in the southwestern region (Zhang et al., 2017). Hence, high priority-management area could be proposed according to the distribution of high-high sites (Zhang et al., 2019). Moreover, the low-low sites for As, Cd, Pb, Sb, and Zn were mainly observed in the north part of Hezhang. Similar to the results of spatial interpolation (Figure 3), As, Cd, Pb, Sb, and Zn diminished with the distance away from the southwest edge. This may imply a significant influence from these industrial activities (Zhao, Zhang, et al., 2020). Additionally, for most sites, the results of the local Moran's I were not significant (Figure 4).

4.3 | Source apportionment

As mentioned above, four factors were extracted by APC-MLR (Figure 5), and five factors were resolved by PMF and UNMIX. Overall, all the factors of PMF were positively correlated ($r = 0.867–0.974$, $p < 0.01$) with those of UNMIX (Table S8). This suggested the occurrence of the same profiles of pollution sources. Although no significant correlations for Factor 1 and Factor 2 of APCS-MLR with their

corresponding factors of PMF or UNMIX, their similar heavy loadings could be attributed to the same source. Despite the low contributions of APCS-MLR and the lack of significant correlation of Factor 3 of APCS-MLR with those of PMF and UNMIX, the heavy loading of Factor 3 of all these receptors was heavily loaded with Cd; it may also be interpreted as a pollution source. Factor 4 of the APCS-MLR had a positive correlation with those of PMF ($r = 0.876$, $p < 0.01$) and UNMIX ($r = 0.848$, $p < 0.01$), and high loadings of Cr were observed for all receptor models. Factor 5 was resolved only in PMF and UNMIX with high loadings of As and Sb indicating a similar source.

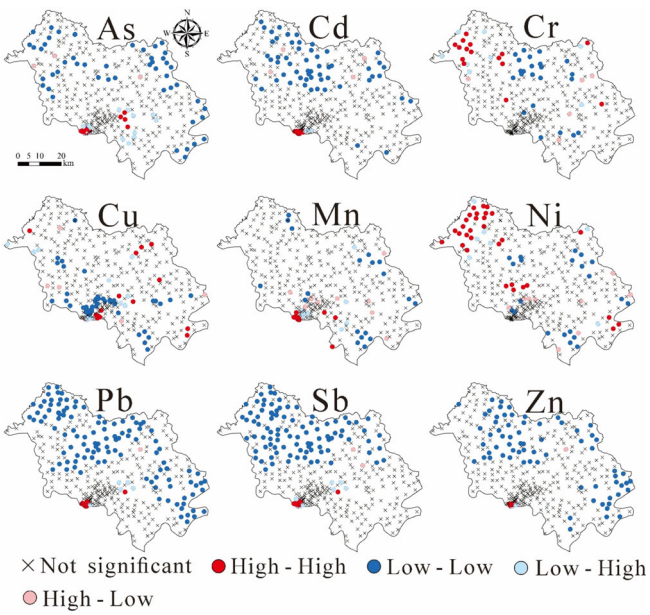

FIGURE 4 Local Moran's I of As, Cd, Cr, Cu, Mn, Ni, Pb, Sb, and Zn [Colour figure can be viewed at wileyonlinelibrary.com]

For APCS-MLR and PMF, Factor 1 was as major contributor (Figure 5), and for UNMIX, Factor 2 was the greatest contributor. Considering the contribution rates and ratios of these different factors, Factor 5 of PMF and UNMIX may be derived from Factor 1 of APCS-MLR.

Factor 1 was mainly loaded with Pb, Sb, and Zn. As mentioned above, Hezhang County is famous for its Pb–Zn mining and smelting activities (Bi et al., 2006). Interestingly, the hotspots of Pb, Zn, As, and Sb coincided with the spatial distribution of Pb–Zn mining, smelting, and cement activities in the southwest regions of Hezhang (Figure 1). As atmospheric precipitation is a dominant source of Pb and Zn, the Pb- and Zn-enriched particles emitted from smelters could impact soil HM concentrations (Xu et al., 2021). The unsuitable disposal of the smelting waste has led to their accumulation in the surrounding environments (Briki et al., 2015). Moreover, in the southwest edge of Hezhang, the cement-related industrial activities with the annual production of 0.536 million tons of cement could substantially contribute to Pb and Zn accumulation in nearby farmlands (Chai et al., 2021; HZBS, 2020). Hence, Factor 1 could be dominated by Pb–Zn mining and other smelting and cement activities. Factor 2 was determined by Cu and Mn. As an inherent component of additives in livestock diets (Guan et al., 2018), Cu could be transferred to animals and then farmland via the common agricultural by-products of manure and cattle slurry (Pan et al., 2016), which are common and necessary agricultural practices in the study area. Moreover, the application of fertilizers and pesticides could also contribute to Cu accumulation in farmland soils (Liang et al., 2017; Wu et al., 2020). Mn, an essential element in crops, is widely included in fertilizers (Deng et al., 2020). Together with the widespread distribution of Cu (Figure 3), hence, we confirmed that Factor 2 could be an agricultural source. Factor 3 was primarily loaded with Cd. Previous studies have proposed that Cd could be released from coal combustion and iron smelting (Guo, Zhang, & Wang, 2021).

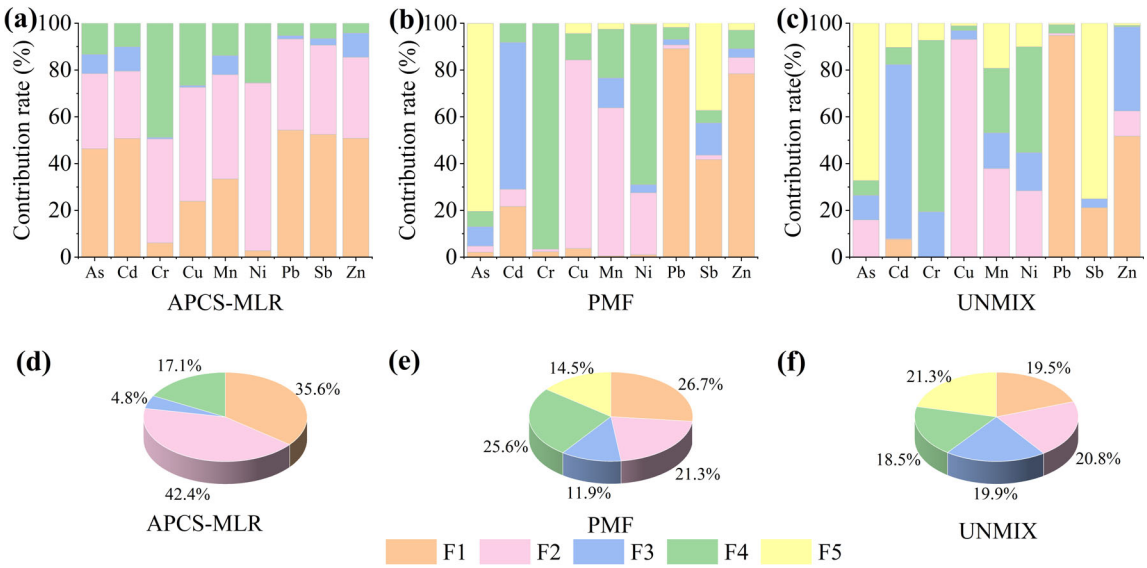

FIGURE 5 Factors contribution by (a) APCS-MLR, (b) PMF, (c) UNMIX; and the overall contributions resolved by (d) APCS-MLR, (e) PMF, and (f) UNMIX [Colour figure can be viewed at wileyonlinelibrary.com]

Given the facts that high amounts of coal mining and iron casting, Factor 3 could be classified as a source occurring from iron smelting and coal burning (HZBS, 2020; HZSY, 2017). Factor 4 was dominated by Cr and Ni. Robust evidence showed that Cr and Ni mainly originated from lithogenic components: they were usually considered as indicators of natural sources (Guo, Zhang, & Wang, 2021; Pan et al., 2016). Considering the high Cr and Ni loadings of Factor 4, thus, Factor 4 represents natural source, including soil parent materials and pedogenesis (Fei et al., 2020). Since Cr and Ni were considered as indicators of natural sources (Guo, Wang, et al., 2021), and the weak relations with the other HM, thus, other HM may originate from anthropogenic sources rather than natural sources. Factor 5 was characterized by As and Sb. As mentioned above, intensive coal mining activities producing approximately 1.11 million tons of coal in Hezhang annually confirmed a high presence of As in coal (Yudovich & Ketris, 2005; Zhao et al., 2008). Since Sb is one of the most mined metal in Hezhang, the associated deposition of Sb in surrounding farmlands is expected (Ao et al., 2019). Furthermore, hotspots of As and Sb were found in the southwestern parts of Hezhang, where most Sb mining and coal mining also occurred (Figures 1 and 3). Thus, Factor 5 could be linked to coal and Sb mining.

All the predicted results of the receptor models were in accordance with the observed values (Table S9). Despite the differences between models in resolving the individual elements, a consensus was reached. UNMIX was more accurate in explaining Cd, Pb, Sb, and Zn, with an r^2 >0.97 and an error percentage ≤2.05%. APCS-MLR was more accurate in resolving Cr, Cu, Mn, and Ni, with an r^2 >0.831 and error percentages ≤5.02%. PMF models were the most accurate in

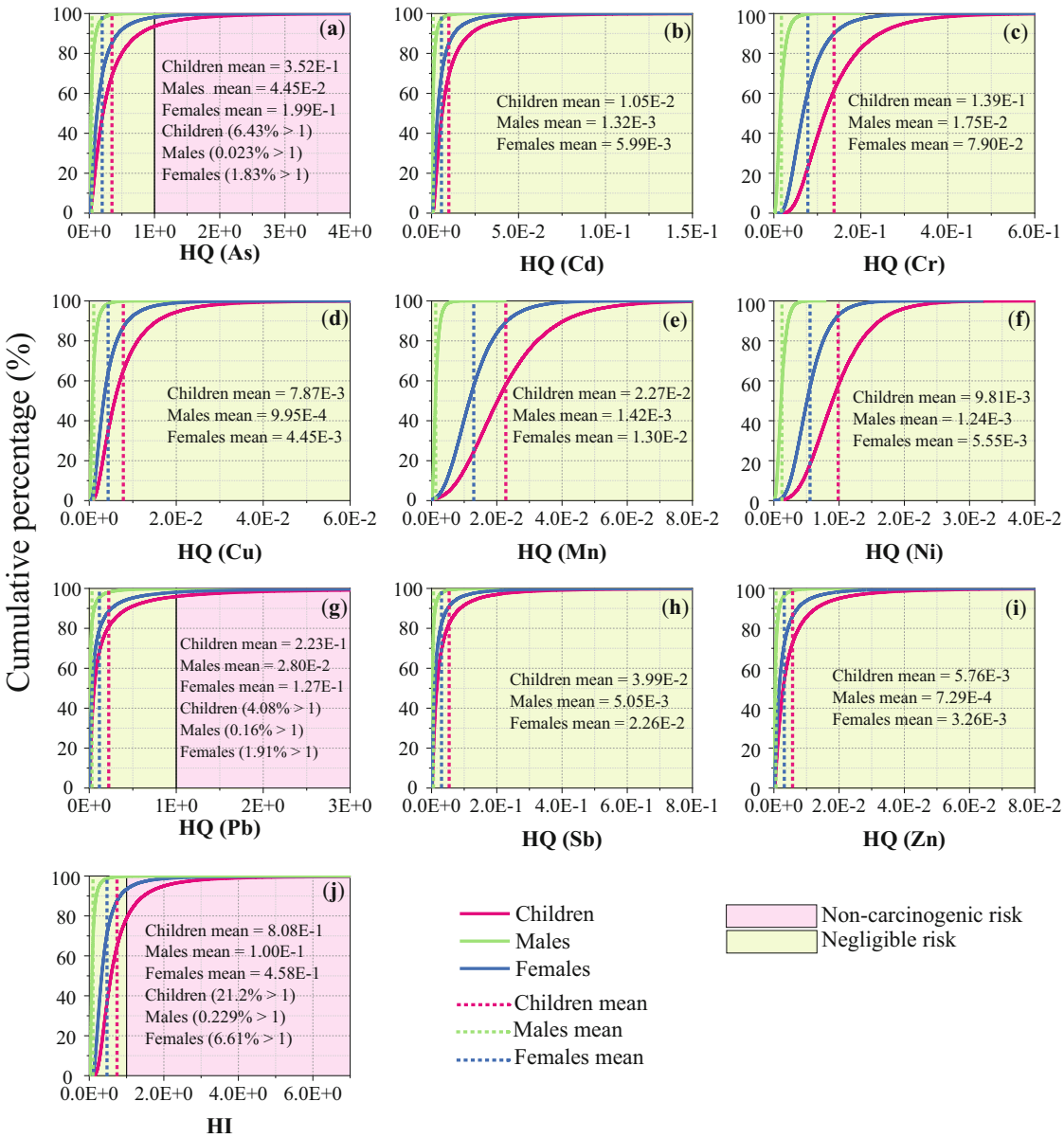

FIGURE 6 Probability distributions for hazard quotient (HQ) of (a) As, (b) Cd, (c) Cr, (d) Cu, (e) Mn, (f) Ni, (g) Pb, (h) Sb, (i) Zn, (j) hazard index (HI). The pink lines represent HQ or HI for children, blue lines for HQ or HI for female (adult), green lines for male (adult) [Colour figure can be viewed at wileyonlinelibrary.com]

explaining the sources of As with $r^2 = 1$ and an error percentage of 3.12%. Owing to the differences in algorithms in the models, differences in source apportionment results were also expected (Guan et al., 2019). Therefore, to obtain more convincing results, different models should be applied simultaneously.

4.4 | Health risk assessment

Although the mean HQ in all categories was <1, high As HQs >1 could be observed in children-6.43%, adult females-1.83%, and adult males-0.023%, respectively (Figure 6). This also indicated that the NCR from As was >1. Similarly, although the mean Pb HQs for children, adult females, and males were <1, the Pb HQs >1 for children, adult females, and adult males were approximately 4.08%, 1.91%, and 0.16%, respectively. This also indicated that the NCR from Pb was >1 (Figure 6). Thus, As and Pb were the dominant contributors to the NCR from HM. As with the individual elements, a similar trend was observed with the mean HI (<1) of children (8.08E-1), adult females (4.58E-1), and adult males (1.00E-1) were <1 (Table S10). However, the 90th percentile of HI for children (21.1%), 95th percentile of adult females (6.61%), and 99.9th percentile of HI for adult males (0.229%) were >1. This indicated that the NCR from these HM was >1.

The contribution of HMs to the CR followed the order of As > Cd > Pb > Cr > Ni. The 75th TCR for children and adult females and the 99th TCR value for adult males were > 1E-4 (Table S11). Specifically, the As CR values for children (47.8%), adult females (27.1%), and adult males (2.10%) were > 1E-4. The Cd CRs for these groups were 16.1%, 6.24%, and 0.212%, respectively. The Pb CRs for these groups were 0.741%, 0.277%, and 0.009%, respectively. Collectively, As, Cd, and Pb were found to be high-priority HMs. Furthermore, the mean TCR of children and adult females was up to 2.33- and 1.32-times higher than the acceptable threshold value of 1E-4 (Figure 7f). Moreover, 100% of TCR values for children and adult females and 99.97% of TCR for adult males were higher than the threshold value of 1E-6. Particularly, 74.9%, 46.6%, and 3.27% of TCR values for children, adult females, and adult males exceeded the acceptable carcinogenic threshold value of 1E-4. Collectively, these data were indicative of the serious CR from HM in farmland soils in Hezhang.

Based on the results of the receptor models (Table S9), the health risks by different sources, including NCR and TCR, were also investigated. Although different exposure levels in different groups, same contribution rates of different factors could be expected due to the same contribution rates to HM in soils (Huang et al., 2021). The total NCR (Figure S7) was dominated by Factor 5 (resolved as coal mining and Sb mining), followed by Factor 1 (Pb–Zn mining and smelting). Moreover, for CR, Factor 5 (57.6%) and Factor 3 (25.7%) had comparably higher contribution rates. Since these factors were heavily loaded with As, Cd, and Pb, these elements were deemed as priority-control HM. In this study, only total concentrations of HM were determined; the form and bioavailability of HM should be taken into account as the toxicity of HM greatly depend on them (Varol et al., 2021).

5 | CONCLUSIONS

Overall, our findings showed that the local GBV of Cd, Cr, Cu, Mn, Ni, Pb, and Zn were greater than the Guizhou Provincecial BV,

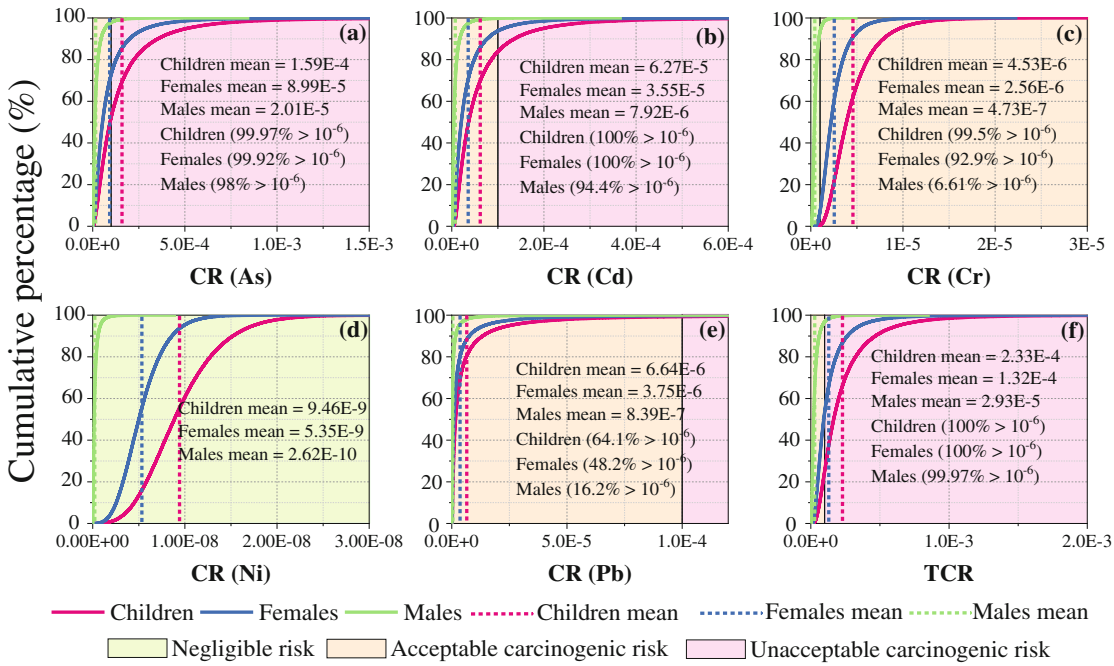

FIGURE 7 Probability distributions for carcinogenic risk (CR) of (a) As, (b) Cd, (c) Cr, (d) Ni, (e) Pb, and (f) total carcinogenic risk (TCR) [Colour figure can be viewed at wileyonlinelibrary.com]

highlighting the necessity to establish regional GBV when conducting regional work in the Karst Plateau regions. Except for Cr, all the other HM clustered in their distribution. The most contaminated sites aggregated on the southwestern edge of Hezhang County. Results of receptor models showed that metal ore mining and smelting, coal mining, cement products activities, and related industrial activities were the main pollution sources in the study area. As, Cd, and Pb were deemed as priority-control HM in farmland soils in the study area, due to the high human exposure risks. The identification of sources and locations can be directly applied by local policymakers for public health protection, land use planning, and risk mitigation.

ACKNOWLEDGMENTS

This work was supported by the National Natural Science Foundation of China, Project of Karst Scientific Research Center of the People's Government of Guizhou Province (U1612442), The Science and Technology Foundation of Guizhou Province: Qiankehe [2020]1Y140, National Key Research and Development Program of China (No. 2020YFC1808500), China Postdoctoral Science Foundation (2019M663571), and National Natural Science Foundation of China (NSFC: 42003065).

CONFLICT OF INTEREST

The authors declare that they have no known competing financial interests or personal relationships that could have appeared to influence the work reported in this paper.

DATA AVAILABILITY STATEMENT

The data that support the findings of this study are available from the corresponding author upon reasonable request.

ORCID

Xiaohang Xu https://orcid.org/0000-0001-7084-3132

REFERENCES

Ahmadi, M., Akhbarizadeh, R., Haghighifard, N. J., Barzegar, G., & Jorfi, S. (2019). Geochemical determination and pollution assessment of heavy metals in agricultural soils of south western of Iran. *Journal of Environmental Health Science and Engineering*, *17*(2), 657–669. https://doi.org/10.1007/s40201-019-00379-6

Ao, M., Qiu, G., Zhang, C., Xu, X., Zhao, L., Feng, X., Qin, S., & Meng, B. (2019). Atmospheric deposition of antimony in a typical mercury-antimony mining area, Shaanxi Province, Southwest China. *Environmental Pollution*, *245*, 173–182. https://doi.org/10.1016/j.envpol.2018.10.125

Balkhair, K. S., & Ashraf, M. A. (2016). Field accumulation risks of heavy metals in soil and vegetable crop irrigated with sewage water in western region of Saudi Arabia. *Saudi Journal of Biological Sciences*, *23*(1), S32–S44. https://doi.org/10.1016/j.sjbs.2015.09.023

Bi, X. Y., Feng, X. B., Yang, Y. G., Qiu, G. L., Li, G. H., Li, F. L., Liu, T., Fu, Z., & Jin, Z. S. (2006). Environmental contamination of heavy metals from zinc smelting areas in Hezhang County, western Guizhou, China. *Environment International*, *32*(7), 883–890. https://doi.org/10.1016/j.envint.2006.05.010

Briki, M., Ji, H. B., Li, C., Ding, H. J., & Gao, Y. (2015). Characterization, distribution, and risk assessment of heavy metals in agricultural soil and products around mining and smelting areas of Hezhang, China. *Environmental Monitoring and Assessment*, *187*(12), 767. https://doi.org/10.1007/s10661-015-4951-2

Brtnický, M., Pecina, V., Hladký, J., Radziemska, M., Koudelková, Z., Klimánek, M., Richtera, L., Adamcová, D., Elbl, J., Galiová, M. V., Baláková, L., Kynický, J., Smolíková, V., Houška, J., & Vaverková, M. D. (2019). Assessment of phytotoxicity, environmental and health risks of historical urban park soils. *Chemosphere*, *220*, 678–686. https://doi.org/10.1016/j.chemosphere.2018.12.188

Chai, L., Wang, Y. H., Wang, X., Ma, L., Cheng, Z. X., & Su, L. M. (2021). Pollution characteristics, spatial distributions, and source apportionment of heavy metals in cultivated soil in Lanzhou, China. *Ecological Indicators*, *125*, 107507. https://doi.org/10.1016/j.ecolind.2021.107507

Chen, F., Wang, Q., Meng, F. L., Chen, M., & Wang, B. (2020). Effects of long-term zinc smelting activities on the distribution and health risk of heavy metals in agricultural soils of Guizhou Province, China. *Environmental Geochemistry and Health*. 1–16. https://doi.org/10.1007/s10653-020-00716-x

Cheng, H., Li, K., Li, M., Yang, K., Liu, F., & Cheng, X. (2014). Geochemical background and baseline value of chemical elements in urban soil in China. *Earth Science Frontiers*, *21*(3), 265–306. https://doi.org/10.13745/j.esf.2014.03.028

Cheng, H. X., Li, M., Zhao, C. D., Li, K., Peng, M., Qin, A. H., & Cheng, X. M. (2014). Overview of trace metals in the urban soil of 31 metropolises in China. *Journal of Geochemical Exploration*, *139*, 31–52. https://doi.org/10.1016/j.gexplo.2013.08.012

CNEMC. (1990). *(the Chinese Environmental Monitoring Centre) the background values of soil elements in China*. Beijing: China Environmental Science Press (in Chinese).

Deng, X., Chen, Y., Yang, Y., Lu, L., Yuan, X., Zeng, H., & Zeng, Q. (2020). Cadmium accumulation in rice (*Oryza sativa* L.) alleviated by basal alkaline fertilizers followed by topdressing of manganese fertilizer. *Environmental Pollution*, *262*, 114289. https://doi.org/10.1016/j.envpol.2020.114289

Duan, Z., Luo, Y., Wu, Y., Wang, J., Cai, X., Wen, J., & Xu, J. (2021). Heavy metals accumulation and risk assessment in a soil-maize (*Zea mays* L.) system around a zinc-smelting area in Southwest China. *Environmental Geochemistry and Health*, *43*(12), 4875–4889. https://doi.org/10.1007/s10653-021-01003-z

Fei, X. F., Lou, Z. H., Xiao, R., Ren, Z. Q., & Lv, X. N. (2020). Contamination assessment and source apportionment of heavy metals in agricultural soil through the synthesis of PMF and GeogDetector models. *Science of the Total Environment*, *747*, 141293. https://doi.org/10.1016/j.scitotenv.2020.141293

Feng, X., Li, G., & Qiu, G. (2004). A preliminary study on mercury contamination to the environment from artisanal zinc smelting using indigenous methods in Hezhang county, Guizhou, China—Part 1: Mercury emission from zinc smelting and its influences on the surface waters. *Atmospheric Environment*, *38*(36), 6223–6230. https://doi.org/10.1016/j.atmosenv.2004.07.020

Fernandez-Caliani, J. C., Romero-Baena, A., Gonzalez, I., & Galan, E. (2020). Geochemical anomalies of critical elements (Be, Co, Hf, Sb, Sc, Ta, V, W, Y and REE) in soils of western Andalusia (Spain). *Applied Clay Science*, *191*, 105610. https://doi.org/10.1016/j.clay.2020.105610

Franco-Uria, A., Lopez-Mateo, C., Roca, E., & Fernandez-Marcos, M. L. (2009). Source identification of heavy metals in pastureland by multivariate analysis in NW Spain. *Journal of Hazardous Materials*, *165*(1–3), 1008–1015. https://doi.org/10.1016/j.jhazmat.2008.10.118

Gebeyehu, H. R., & Bayissa, L. D. (2020). Levels of heavy metals in soil and vegetables and associated health risks in Mojo area, Ethiopia. *PLoS One*, *15*(1), e0227883. https://doi.org/10.1371/journal.pone.0227883

Ginsberg, G. L., & Belleggia, G. (2017). Use of Monte Carlo analysis in a risk-based prioritization of toxic constituents in house dust. *Environment International*, *109*, 101–113. https://doi.org/10.1016/j.envint.2017.06.009

Guan, Q., Zhao, R., Pan, N., Wang, F., Yang, Y., & Luo, H. (2019). Source apportionment of heavy metals in farmland soil of Wuwei, China: Comparison of three receptor models. *Journal of Cleaner Production*, *237*, 117792. https://doi.org/10.1016/j.jclepro.2019.117792

Guan, Q. Y., Wang, F. F., Xu, C. Q., Pan, N. H., Lin, J. K., Zhao, R., Yang, Y., & Luo, H. P. (2018). Source apportionment of heavy metals in agricultural soil based on PMF: A case study in Hexi Corridor, Northwest China. *Chemosphere*, *193*, 189–197. https://doi.org/10.1016/j.chemosphere.2019.125272

Guo, G. H., Wang, Y. T., Zhang, D. G., & Lei, M. (2021). Source-specific ecological and health risks of potentially toxic elements in agricultural soils in southern Yunnan Province and associated uncertainty analysis. *Journal of Hazardous Materials*, *417*, 126144. https://doi.org/10.1016/j.jhazmat.2021.126144

Guo, G. H., Zhang, D. G., & Wang, Y. (2021). Source apportionment and source-specific health risk assessment of heavy metals in size-fractionated road dust from a typical mining and smelting area, Gejiu, China. *Environmental Science and Pollution Research*, *28*(8), 9313–9326. https://doi.org/10.1007/s11356-020-11312-y

Guo, H., Wang, T., & Louie, P. K. K. (2004). Source apportionment of ambient non-methane hydrocarbons in Hong Kong: Application of a principal component analysis/absolute principal component scores (PCA/APCS) receptor model. *Environmental Pollution*, *129*(3), 489–498. https://doi.org/10.1016/j.envpol.2003.11.006

Hani, A., & Pazira, E. (2011). Heavy metals assessment and identification of their sources in agricultural soils of southern Tehran, Iran. *Environmental Monitoring and Assessment*, *176*(1–4), 677–691. https://doi.org/10.1007/s10661-010-1612-3

Hou, D. Y., O'Connor, D., Nathanail, P., Tian, L., & Ma, Y. (2017). Integrated GIS and multivariate statistical analysis for regional scale assessment of heavy metal soil contamination: A critical review. *Environmental Pollution*, *231*, 1188–1200. https://doi.org/10.1016/j.envpol.2017.07.021

Hu, B., Jia, X., Hu, J., Xu, D., Xia, F., & Li, Y. (2017). Assessment of heavy metal pollution and health risks in the soil-plant-human system in the Yangtze River Delta, China. *International Journal of Environmental Research and Public Health*, *14*(9), 1042. https://doi.org/10.3390/ijerph14091042

Hu, W. Y., Wang, H. F., Dong, L. R., Huang, B. A., Borggaard, O. K., Bruun Hansen, H. C., He, Y., & Holm, P. E. (2018). Source identification of heavy metals in peri-urban agricultural soils of Southeast China: An integrated approach. *Environmental Pollution*, *237*, 650–661. https://doi.org/10.1016/j.envpol.2018.02.070

Hu, Y., He, K., Sun, Z., Chen, G., & Cheng, H. (2020). Quantitative source apportionment of heavy metal(loid)s in the agricultural soils of an industrializing region and associated model uncertainty. *Journal of Hazardous Materials*, *391*, 122244. https://doi.org/10.1016/j.jhazmat.2020.122244

Hu, Y. N., Cheng, H. F., & Tao, S. (2016). The challenges and solutions for cadmium-contaminated rice in China: A critical review. *Environment International*, *92-93*, 515–532. https://doi.org/10.1016/j.envint.2016.04.042

Huang, J. L., Wu, Y. Y., Sun, J. X., Li, X., Geng, X. L., Zhao, M. L., Sun, T., & Fan, Z. Q. (2021). Health risk assessment of heavy metal(loid)s in park soils of the largest megacity in China by using Monte Carlo simulation coupled with positive matrix factorization model. *Journal of Hazardous Materials*, *415*, 125629. https://doi.org/10.1016/j.jhazmat.2021.125629

HZBS (2020). Statistical Communique on the 2020 National Economy and Social Development of Hezhang County. http://www.gzhezhang.gov.cn.

HZSY. (2017). *Hezhang statistics yearbook*. Dehong, Yunnan Province, China: Dehong Ethnic Publishing House.

Jafarabadi, A. R., Raudonyte-Svirbutaviciene, E., Toosi, A. S., & Bakhtiari, A. R. (2021). Positive matrix factorization receptor model and dynamics in fingerprinting of potentially toxic metals in coastal ecosystem sediments at a large scale (Persian Gulf, Iran). *Water Research*, *188*, 116509. https://doi.org/10.1016/j.watres.2020.116509

Jia, X. L., Hu, B. F., Marchant, B., Zhou, L. Q., Shi, Z., & Zhu, Y. W. (2019). A methodological framework for identifying potential sources of soil heavy metal pollution based on machine learning: A case study in the Yangtze Delta, China. *Environmental Pollution*, *250*, 601–609. https://doi.org/10.1016/j.envpol.2019.04.047

Jiang, H. H., Cai, L. M., Wen, H. H., & Luo, J. (2020). Characterizing pollution and source identification of heavy metals in soils using geochemical baseline and PMF approach. *Scientific Reports*, *10*(1), 6460. https://doi.org/10.1038/s41598-020-63604-5

Jiang, Z. C., Guo, Z. H., Peng, C., Liu, X., Zhou, Z. R., & Xiao, X. Y. (2021). Heavy metals in soils around non-ferrous smelteries in China: Status, health risks and control measures. *Environmental Pollution*, *282*, 117038. https://doi.org/10.1016/j.envpol.2021.117038

Jin, Y. L., O'Connor, D., Ok, Y. S., Tsang, D. C. W., Liu, A., & Hou, D. Y. (2019). Assessment of sources of heavy metals in soil and dust at children's playgrounds in Beijing using GIS and multivariate statistical analysis. *Environment International*, *124*, 320–328. https://doi.org/10.1016/j.envint.2019.01.024

Kamani, H., Mirzaei, N., Ghaderpoori, M., Bazrafshan, E., Rezaei, S., & Mahvi, A. H. (2018). Concentration and ecological risk of heavy metal in street dusts of Eslamshahr, Iran. *Human and Ecological Risk Assessment: An International Journal*, *24*(4), 961–970. https://doi.org/10.1080/10807039.2017.1403282

Karim, Z., Qureshi, B. A. L., & Mumtaz, M. (2015). Geochemical baseline determination and pollution assessment of heavy metals in urban soils of Karachi, Pakistan. *Ecological Indicators*, *48*, 358–364. https://doi.org/10.1016/j.ecolind.2014.08.032

Li, C. C., Huo, S. L., Yu, Z. Q., Xi, B. D., Zeng, X. Y., & Wu, F. C. (2014). Spatial distribution, potential risk assessment, and source apportionment of polycyclic aromatic hydrocarbons (PAHs) in sediments of Lake Chaohu, China. *Environmental Science and Pollution Research*, *21*(20), 12028–12039. https://doi.org/10.1007/s11356-014-3137-8

Li, J., Xu, X., Lv, J., Wu, Q., Ren, M., Cao, J., & Liu, P. (2020). Source apportionment and health risk quantification for heavy metal sources in soils near aluminum-plastic manufacturing facilities in Northeast China. *Human and Ecological Risk Assessment: An International Journal*, *26*(8), 2225–2244. https://doi.org/10.1080/10807039.2019.1669430

Li, N., Kang, Y., Pan, W. J., Zeng, L. X., Zhang, Q. Y., & Luo, J. W. (2015). Concentration and transportation of heavy metals in vegetables and risk assessment of human exposure to bioaccessible heavy metals in soil near a waste-incinerator site, South China. *Science of the Total Environment*, *521*, 144–151. https://doi.org/10.1016/j.scitotenv.2015.03.081

Li, Y. H., Kuang, H. F., Hu, C. H., & Ge, G. (2021). Source apportionment of heavy metal pollution in agricultural soils around the Poyang Lake region using UNMIX model. *Sustainability*, *13*(9), 5272. https://doi.org/10.3390/su13095272

Lian, M., Wang, J., Sun, L., Xu, Z., Tang, J., Yan, J., & Zeng, X. (2019). Profiles and potential health risks of heavy metals in soil and crops from the watershed of Xi River in Northeast China. *Ecotoxicology and Environmental Safety*, *169*, 442–448. https://doi.org/10.1016/j.ecoenv.2018.11.046

Liang, J., Feng, C. T., Zeng, G. M., Gao, X., Zhong, M. Z., Li, X. D., Li, X., He, X., & Fang, Y. L. (2017). Spatial distribution and source identification of heavy metals in surface soils in a typical coal mine city, Lianyuan, China. *Environmental Pollution*, *225*, 681–690. https://doi.org/10.1016/j.envpol.2017.03.057

Liu, J., Liu, Y. J., Liu, Y., Liu, Z., & Zhang, A. N. (2018). Quantitative contributions of the major sources of heavy metals in soils to ecosystem and human health risks: A case study of Yulin, China. *Ecotoxicology and*

Environmental Safety, *164*, 261–269. https://doi.org/10.1016/j.ecoenv.2018.08.030

Liu, L. L., Dong, Y. C., Kong, M., Zhou, J., Zhao, H. B., Tang, Z., Zhang, M., & Wang, Z. P. (2020). Insights into the long-term pollution trends and sources contributions in Lake Taihu, China using multi-statistic analyses models. *Chemosphere*, *242*, 125272. https://doi.org/10.1016/j.chemosphere.2019.125272

Liu, P., Wu, Z., Luo, X., Wen, M., Huang, L., Chen, B., Zheng, C., Zhu, C., & Liang, R. (2020). Pollution assessment and source analysis of heavy metals in acidic farmland of the karst region in southern China—A case study of Quanzhou County. *Applied Geochemistry*, *123*, 104764. https://doi.org/10.1016/j.apgeochem.2020.104764

Long, Z., Zhu, H., Bing, H., Tian, X., Wang, Z., Wang, X., & Wu, Y. (2021). Contamination, sources and health risk of heavy metals in soil and dust from different functional areas in an industrial city of Panzhihua City, Southwest China. *Journal of Hazardous Materials*, *420*, 126638. https://doi.org/10.1016/j.jhazmat.2021.126638

Lu, X. Z., Gu, A. Q., Huang, C. L., Wei, Y. C., Xu, M. X., Yin, H. Q., & Hu, X. F. (2021). Assessments of heavy metal pollution of a farmland in an urban area based on the environmental geochemical baselines. *Journal of Soils and Sediments*, *21*(7), 2659–2671. https://doi.org/10.1007/s11368-021-02945-8

Luo, C. L., Liu, C. P., Wang, Y., Liu, X. A., Li, F. B., Zhang, G., & Li, X. D. (2011). Heavy metal contamination in soils and vegetables near an e-waste processing site, South China. *Journal of Hazardous Materials*, *186*(1), 481–490. https://doi.org/10.1016/j.jhazmat.2010.11.024

Mehr, M. R., Keshavarzi, B., Moore, F., Sharifi, R., Lahijanzadeh, A., & Kermani, M. (2017). Distribution, source identification and health risk assessment of soil heavy metals in urban areas of Isfahan Province, Iran. *Journal of African Earth Sciences*, *132*, 16–26. https://doi.org/10.1016/j.jafrearsci.2017.04.026

MEPRC (2018). (Ministry of Environmental Protection of the People's Republic of China) soil environmental quality risk of control standard for soil contamination of agricultural land (GB15618-2018). Ministry of Environmental Protection of the People's Republic of China.

Mico, C., Peris, M., Recatala, L., & Sanchez, J. (2007). Baseline values for heavy metals in agricultural soils in an European Mediterranean region. *Science of the Total Environment*, *378*(1–2), 13–17. https://doi.org/10.1016/j.scitotenv.2007.01.010

Mohammad, H. G., Melesse, A. M., & Reddi, L. (2016). Water quality assessment and apportionment of pollution sources using APCS-MLR and PMF receptor modeling techniques in three major rivers of South Florida. *Science of the Total Environment*, *566-567*, 1552–1567. https://doi.org/10.1016/j.scitotenv.2016.06.046

MohseniBandpi, A., Eslami, A., Ghaderpoori, M., Shahsavani, A., Jeihooni, A. K., Ghaderpoury, A., & Alinejad, A. (2018). Health risk assessment of heavy metals on PM2.5 in Tehran air, Iran. *Data in Brief*, *17*, 347–355. https://doi.org/10.1016/j.dib.2018.01.018

Niu, L. L., Yang, F. X., Xu, C., Yang, H. Y., & Liu, W. P. (2013). Status of metal accumulation in farmland soils across China: From distribution to risk assessment. *Environmental Pollution*, *176*, 55–62. https://doi.org/10.1016/j.envpol.2013.01.019

Niu, S. P., Gao, L. M., & Wang, X. (2019). Characterization of contamination levels of heavy metals in agricultural soils using geochemical baseline concentrations. *Journal of Soils and Sediments*, *19*(4), 1697–1707. https://doi.org/10.1007/s11368-018-2190-1

Pan, L. B., Ma, J., Wang, X. L., & Hou, H. (2016). Heavy metals in soils from a typical county in Shanxi Province, China: Levels, sources and spatial distribution. *Chemosphere*, *148*, 248–254. https://doi.org/10.1016/j.chemosphere.2015.12.049

Qin, W., Han, D., Song, X., & Liu, S. (2021). Sources and migration of heavy metals in a karst water system under the threats of an abandoned Pb–Zn mine, Southwest China. *Environmental Pollution*, *277*, 116774. https://doi.org/10.1016/j.envpol.2021.116774

Rinklebe, J., Shaheen, S. M., El-Naggar, A., Wang, H. L., Du Laing, G., Alessi, D. S., & Ok, Y. S. (2020). Redox-induced mobilization of ag, Sb, Sn, and Tl in the dissolved, colloidal and solid phase of a biochar-treated and un-treated mining soil. *Environment International*, *140*, 105754. https://doi.org/10.1016/j.envint.2020.105754

Sakizadeh, M., & Zhang, C. S. (2021). Source identification and contribution of land uses to the observed values of heavy metals in soil samples of the border between Northern Ireland and Republic of Ireland by receptor models and redundancy analysis. *Geoderma*, *404*, 115313. https://doi.org/10.1016/j.geoderma.2021.115313

Shaheen, S. M., Antoniadis, V., Kwon, E., Song, H., Wang, S. L., Hseu, Z. Y., & Rinklebe, J. (2020). Soil contamination by potentially toxic elements and the associated human health risk in geo- and anthropogenic contaminated soils: A case study from the temperate region (Germany) and the arid region (Egypt). *Environmental Pollution*, *262*, 114312. https://doi.org/10.1016/j.envpol.2020.114312

Shen, D., Huang, S., Zhang, Y., & Zhou, Y. (2021). The source apportionment of N and P pollution in the surface waters of lowland urban area based on EEM-PARAFAC and PCA-APCS-MLR. *Environmental Research*, *197*, 111022. https://doi.org/10.1016/j.envres.2021.111022

Sun, L., Guo, D. K., Liu, K., Meng, H., Zheng, Y. J., Yuan, F. Q., & Zhu, G. H. (2019). Levels, sources, and spatial distribution of heavy metals in soils from a typical coal industrial city of Tangshan, China. *Catena*, *175*, 101–109. https://doi.org/10.1016/j.catena.2018.12.014

Tepanosyan, G., Sahakyan, L., Zhang, C. S., & Saghatelyan, A. (2019). The application of local Moran's I to identify spatial clusters and hot spots of Pb, Mo and Ti in urban soils of Yerevan. *Applied Geochemistry*, *104*, 116–123. https://doi.org/10.1016/j.apgeochem.2019.03.022

Tian, K., Huang, B., Xing, Z., & Hu, W. Y. (2017). Geochemical baseline establishment and ecological risk evaluation of heavy metals in greenhouse soils from Dongtai, China. *Ecological Indicators*, *72*, 510–520. https://doi.org/10.1016/j.ecolind.2016.08.037

USEPA (2001). Risk Assessment Guidance for Superfund: Volume III - Part A, Process for conducting probabilistic risk assessment. https://www.epa.gov/risk/risk-assessment-guidance-superfund-rags-volume-iii-part. (Last accessible March 25, 2022)

USEPA (2009). (United States environmental protection agency) risk assessment guidance for superfund (RAGS), volume I, human health evaluation manual (part E, supplemental guidance for dermal risk assessment). https://www.epa.gov/risk/risk-assessment-guidance-superfund-rags-part-e (Last accessible March 25, 2022)

Varol, M., Gündüz, K., & Sünbül, M. R. (2021). Pollution status, potential sources and health risk assessment of arsenic and trace metals in agricultural soils: A case study in Malatya Province, Turkey. *Environmental Research*, *202*, 111806. https://doi.org/10.1016/j.envres.2021.111806

Wang, F., Guan, Q., Tian, J., Lin, J., Yang, Y., Yang, L., & Pan, N. (2020). Contamination characteristics, source apportionment, and health risk assessment of heavy metals in agricultural soil in the Hexi Corridor. *Catena*, *191*, 104573. https://doi.org/10.1016/j.catena.2020.104573

Wang, S. H., Wang, W. W., Chen, J. Y., Zhao, L., Zhang, B., & Jiang, X. (2019). Geochemical baseline establishment and pollution source determination of heavy metals in lake sediments: A case study in Lihu Lake, China. *Science of the Total Environment*, *657*, 978–986. https://doi.org/10.1016/j.scitotenv.2018.12.098

Wang, X., Zhou, J., Xu, S., Chi, Q., Nie, L., Zhang, B., Yao, W., Wang, W., Liu, H., Liu, D., Han, Z., & Liu, Q. (2016). China soil geochemical baselines networks: Data characteristics. *Geology in China*, *43*(5), 1469–1480. https://doi.org/10.12029/gc20160501

Wang, Y. T., Guo, G. H., Zhang, D. G., & Lei, M. (2021). An integrated method for source apportionment of heavy metal(loid)s in agricultural soils and model uncertainty analysis. *Environmental Pollution*, *276*, 116666. https://doi.org/10.1016/j.envpol.2021.116666

Wedepohl, K. H. (1995). The composition of the continental-crust. *Geochimica et Cosmochimica Acta*, *59*(7), 1217–1232. https://doi.org/10.1016/0016-7037(95)00038-2

Wei, C. Y., & Wen, H. L. (2012). Geochemical baselines of heavy metals in the sediments of two large freshwater lakes in China: Implications for contamination character and history. *Environmental Geochemistry and Health*, *34*(6), 737–748. https://doi.org/10.1007/s10653-012-9492-9

Wu, J., Li, J., Teng, Y. G., Chen, H. Y., & Wang, Y. Y. (2020). A partition computing-based positive matrix factorization (PC-PMF) approach for the source apportionment of agricultural soil heavy metal contents and associated health risks. *Journal of Hazardous Materials*, *388*, 121766. https://doi.org/10.1016/j.jhazmat.2019.121766

Wu, Q. M., Hu, W. Y., Wang, H. F., Liu, P., Wang, X. K., & Huang, B. A. (2021). Spatial distribution, ecological risk and sources of heavy metals in soils from a typical economic development area, southeastern China. *Science of the Total Environment*, *780*, 146557. https://doi.org/10.1016/j.scitotenv.2021.146557

Wu, S. H., Zhou, S. L., Bao, H. J., Chen, D. X., Wang, C. H., Li, B. J., Tong, G., Yuan, Y., & Xu, B. G. (2019). Improving risk management by using the spatial interaction relationship of heavy metals and PAHs in urban soil. *Journal of Hazardous Materials*, *364*, 108–116. https://doi.org/10.1016/j.jhazmat.2018.09.094

Xie, W. S., Peng, C., Wang, H. T., & Chen, W. P. (2018). Bioaccessibility and source identification of heavy metals in agricultural soils contaminated by mining activities. *Environmental Earth Sciences*, *77*(17), 606. https://doi.org/10.1007/s12665-018-7783-x

Xu, D. M., Fu, R. B., Liu, H. Q., & Guo, X. P. (2021). Current knowledge from heavy metal pollution in Chinese smelter contaminated soils, health risk implications and associated remediation progress in recent decades: A critical review. *Journal of Cleaner Production*, *286*, 124989. https://doi.org/10.1016/j.jclepro.2020.124989

Xu, X. H., Han, J. L., Pang, J., Wang, X., Lin, Y., Wang, Y. J., & Qiu, G. L. (2020). Methylmercury and inorganic mercury in Chinese commercial rice: Implications for overestimated human exposure and health risk. *Environmental Pollution*, *258*, 113706. https://doi.org/10.1016/j.envpol.2019.113706

Yadav, I. C., Devi, N. L., Singh, V. K., Li, J., & Zhang, G. (2019). Spatial distribution, source analysis, and health risk assessment of heavy metals contamination in house dust and surface soil from four major cities of Nepal. *Chemosphere*, *218*, 1100–1113. https://doi.org/10.1016/j.chemosphere.2018.11.202

Yang, Y. G., Liu, C. Q., Pan, W. U., Zhang, G. P., & Zhu, W. H. (2006). Heavy metal accumulation from zinc smelters in a carbonate rock region in Hezhang County, Guizhou Province, China. *Water, Air, & Soil Pollution*, *174*(1/4), 321–339. https://doi.org/10.1007/s11270-006-9121-2

Yuan, Y. M., Cave, M., & Zhang, C. S. (2018). Using local Moran's I to identify contamination hotspots of rare earth elements in urban soils of London. *Applied Geochemistry*, *88*, 167–178. https://doi.org/10.1016/j.apgeochem.2017.07.011

Yudovich, Y. E., & Ketris, M. P. (2005). Arsenic in coal: A review. *International Journal of Coal Geology*, *61*(3–4), 141–196. https://doi.org/10.1016/j.coal.2004.09.003

Zhan, J., Li, X., Christie, P., & Wu, L. (2021). A review of soil potentially toxic element contamination in typical karst regions in Southwest China. *Current Opinion in Environmental Science & Health*, *23*, 100284. https://doi.org/10.1016/j.coesh.2021.100284

Zhang, J. C., Zhang, Z. M., & Huang, X. F. (2021). Spatial heterogeneity of pH and heavy metal Cd in the soils of tea gardens in the plateau mountain regions, PR China. *Environmental Monitoring and Assessment*, *193*(10), 1–12. https://doi.org/10.1007/s10661-021-09431-1

Zhang, M., Wang, J. M., & Li, S. J. (2019). Tempo-spatial changes and main anthropogenic influence factors of vegetation fractional coverage in a large-scale opencast coal mine area from 1992 to 2015. *Journal of Cleaner Production*, *232*, 940–952. https://doi.org/10.1016/j.jclepro.2019.05.334

Zhang, S., Song, J., Lv, M., & Cheng, Y. (2017). Dietary intake risks of trace metal(loid)s via maize–animal–human pathway and derivation of bioavailability-based soil criteria in Hezhang County, China. *Journal of Soils and Sediments*, *18*(5), 1925–1934. https://doi.org/10.1007/s11368-017-1895-x

Zhang, W. H., Yan, Y., Yu, R. L., & Hu, G. R. (2021). The sources-specific health risk assessment combined with APCS/MLR model for heavy metals in tea garden soils from South Fujian Province, China. *Catena*, *203*, 105306. https://doi.org/10.1016/j.catena.2021.105306

Zhao, K. L., Zhang, L. Y., Dong, J. Q., Wu, J. S., Ye, Z. Q., Zhao, W. M., Ding, L., & Fu, W. J. (2020). Risk assessment, spatial patterns and source apportionment of soil heavy metals in a typical Chinese hickory plantation region of southeastern China. *Geoderma*, *360*, 114011. https://doi.org/10.1016/j.geoderma.2019.114011

Zhao, L., Yan, Y., Yu, R., Hu, G., Cheng, Y., & Huang, H. (2020). Source apportionment and health risks of the bioavailable and residual fractions of heavy metals in the park soils in a coastal city of China using a receptor model combined with Pb isotopes. *Catena*, *194*, 104736. https://doi.org/10.1016/j.catena.2020.104736

Zhao, Y. C., Zhang, J. Y., Huang, W. C., Wang, Z. H., Li, Y., Song, D. Y., Zhao, F., & Zheng, C. G. (2008). Arsenic emission during combustion of high arsenic coals from southwestern Guizhou, China. *Energy Conversion and Management*, *49*(4), 615–624. https://doi.org/10.1016/j.enconman.2007.07.044

Zhou, Y. T., Wang, L. L., Xiao, T. F., Chen, Y. H., Beiyuan, J. Z., She, J. Y., Zhou, Y., Yin, M., Liu, J., Liu, Y., Wang, Y., & Wang, J. (2020). Legacy of multiple heavy metal(loid)s contamination and ecological risks in farmland soils from a historical artisanal zinc smelting area. *Science of the Total Environment*, *720*, 137541. https://doi.org/10.1016/j.scitotenv.2020.137541

SUPPORTING INFORMATION

Additional supporting information may be found in the online version of the article at the publisher's website.

How to cite this article: Han, J., Liang, L., Zhu, Y., Xu, X., Wang, L., Shang, L., Wu, P., Wu, Q., Qian, X., Qiu, G., & Feng, X. (2022). Heavy metal(loid)s in farmland soils on the Karst Plateau, Southwest China: An integrated analysis of geochemical baselines, source apportionment, and associated health risk. *Land Degradation & Development*, *33*(10), 1689–1703. https://doi.org/10.1002/ldr.4257